Quantitative analysis of differential pathlength factor in optical brain imaging under clinical conditions

Lei Wang[1], Hasan Ayaz[2,3,4,5,6], Meltem Izzetoglu[7]

[1]College of Computing and Informatics, Drexel University, Philadelphia, PA, USA
[2]School of Biomedical Engineering, Science and Health Systems, Drexel University, Philadelphia, PA, USA
[3]Department of Psychology, College of Arts and Sciences, Drexel University, Philadelphia, PA
[4]Drexel Solutions Institute, Drexel University, Philadelphia, PA
[5]Department of Family and Community Health, University of Pennsylvania, Philadelphia, PA, USA
[6]Center for Injury Research and Prevention, Children's Hospital of Philadelphia, Philadelphia, PA, USA
[7]Electrical and Computer Engineering, Villanova University, Villanova University, PA, USA

Introduction

Near Infrared Spectroscopy (NIRS) is an optical neuroimaging modality which allows investigation of tissue oxygenation. It is widely utilized to measure cortical oxygenated and deoxygenated hemoglobin concentration changes [1]. With light sources and light detectors placed over the scalp, alterations in light intensities at different wavelengths are recorded, and converted to hemoglobin concentration changes via modified Beer-Lambert law (MBLL) [2]. Differential pathlength factor (DPF) is the ratio of mean optical pathlength the light travel within the tissue to the light source-detector separation distance, which is usually treated as a constant known a priori in MBLL [3]. Our previous study revealed DPF values are dependent on source-detector separations, and detector surface area affects the stability of DPF values. Such variability on DPF values may further lead to inaccurate estimation of hemoglobin concentration in NIRS measurements [3]. The first NIRS clinical studies on newborns and adult cerebrovascular patients were published in 1980s [4, 5]. Through the 1990s and later, the ability of NIRS in detecting intracranial hematomas marked the beginning of clinical application of NIRS for traumatic brain injury (TBI) [5-8]. As NIRS gets widely adopted in clinical studies to acquire accurate brain measurements, the choice of DPF values requires careful evaluation. Several methods have been developed to explain and estimate light propagation and DPF values in highly diffusive media such as human tissue. Monte Carlo (MC) simulation is a stochastics approximation model of Radiative Transfer Equation (RTE), which offers excellent accuracy when simulating photon propagation inside general complex media. Due to its flexibility and recent advances in computational speed, the MC method has been explored in tissue optics to solve both the forward and inverse problems in many studies [3, 9-20]. In this study, we investigated the contributing factors on DPF values, DPF values under clinical conditions using digital head models in MC simulations.

Methods:

A three-dimensional digital head model with four-layer slab geometry (150 x 150 x 60 mm^3) was designed to monitor adult head with three separate clinical cases (intracranial hematoma, cerebral edema and perihematomal edema). The thickness of each layer was designed as: 3 mm of scalp, 7 mm of skull, 2 mm of cerebrospinal fluid (CSF), and 48 mm of brain tissue [21]. Lesion of each case was modeled as a 10-mm-tall cylinder, and presented within the brain tissue layer, on the midline between source and detector, with increased radius (9.77 mm, 12.62 mm, 17.84 mm and 30.90 mm), resulting in 3 cc, 5 cc, 10 cc and 30 cc lesion volumes. For perihematomal edema case, volume of blood to water is 1:1. Each lesion type and

size was placed at different depths within the brain layer: 0.5 mm, 3 mm, 5.5 mm and 8 mm, resulting the lesion to skin surface being 12.5 mm, 15 mm, 17.5 mm and 20 mm (See Figure 1.a). Optical properties assigned to each tissue type for MC simulation were as shown in Table 1, corresponding to wavelength at 830 nm [3, 22]. For each source-detector separation of 10 mm, 15 mm, 20 mm, 25 mm, 30 mm, 35 mm and 40 mm, 10 random simulations were conducted, 100 million photons were launched per simulation. Light detectors were modeled as a disk with a radius of 1.2 mm, based on previous investigation on detector surface area [3]. DPFs obtained from simulations under different conditions were compared to healthy condition and evaluated with various source-detector separations.

Results:

The MC simulated DPFs indicated that the DPF changes with the type of lesion (See Figure 1.b). Moreover, DPF values are lower than healthy for lesions such as intracranial hematoma and perihematomal edema. As the lesions presented at the same depth within the brain layer, but with increasing volumes, DPFs are getting much lower than healthy conditions. When the lesion volumes are the same, but presented at different depths in the brain, the closer the lesion to the light source, the smaller the DPFs. Results from cerebral edema simulations revealed a different pattern. Increasing the lesion volumes will lead to higher DPFs compared to healthy condition. As the edema presented deeper in the brain, DPFs are getting smaller. The difference in DPFs between clinical models and healthy conditions are more pronounced with larger source-detector separations.

Discussion:

The simulated DPFs from digital head models with various clinical conditions revealed that, in addition to the source-detector separation and detector surface area, DPFs are also dependent on the following factors: the depth of the lesion present in the brain, the volume size of the lesion, as well as the type of the lesion. Early investigation also indicated that DPFs are affected by wavelength and subject age [23]. With such a clear quantitative comparison on simulated DPFs, a more accurate DPF estimation can be performed to obtain more reliable hemoglobin concentration calculation for NIRS clinical studies. This quantitative analysis and DPF results highlight the potential to optimize optical brain imaging further by customizing the DPF in order to improve detection and monitoring of brain lesions in the future.

Table 1. Tissue optical properties in clinical digital head phantom. Anisotropy g = 0.9, and refractive index n = 1.4 in all tissues.

	Scalp	**Skull**	**CSF**	**Brain**	**Blood**	**Water**
μ_a(/mm)	0.0199	0.0141	0.0026	0.0193	0.72	0.0031
μ_s(/mm)	6.47	8.43	0.1	10.88	6.49	0.1

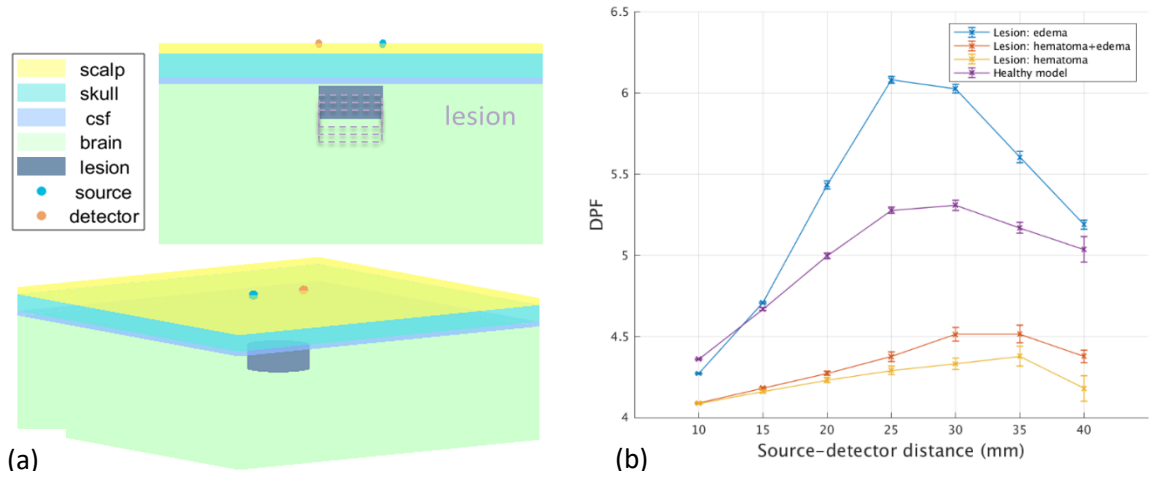

Figure 1. (a) Geometry of digital head model for MC simulation

(b) Simulated DPFs of different lesion types at the same depth (12.5 mm to skin surface) in brain with the same lesion volume (10 cc).

References:

1. Villringer, A. and B. Chance, *Non-invasive optical spectroscopy and imaging of human brain function.* Trends in neurosciences, 1997. **20**(10): p. 435-442.
2. Ayaz, H., et al., *Optical brain monitoring for operator training and mental workload assessment.* Neuroimage, 2012. **59**(1): p. 36-47.
3. Wang, L., et al., *Evaluation of light detector surface area for functional Near Infrared Spectroscopy.* Computers in biology and medicine, 2017. **89**: p. 68-75.
4. Brazy, J.E., et al., *Noninvasive Monitoring of Cerebral Oxygenation in Preterm Infants: Preliminary Observations.* Pediatrics, 1985. **75**(2): p. 217.
5. Sen, A.N., S.P. Gopinath, and C.S. Robertson, *Clinical application of near-infrared spectroscopy in patients with traumatic brain injury: a review of the progress of the field.* Neurophotonics, 2016. **3**(3): p. 031409.
6. Gopinath, S.P., et al., *Near-infrared spectroscopic localization of intracranial hematomas.* Journal of neurosurgery, 1993. **79**(1): p. 43-47.
7. Shankar, P.G., et al., *Early detection of delayed traumatic intracranial hematomas using near-infrared spectroscopy.* Journal of Neurosurgery, 1995. **83**(3): p. 438-444.
8. Ayaz, H., et al., *Early diagnosis of traumatic intracranial hematomas.* Journal of Biomedical Optics, 2019. **24**(5): p. 051411.
9. Kienle, A., et al., *Spatially resolved absolute diffuse reflectance measurements for noninvasive determination of the optical scattering and absorption coefficients of biological tissue.* Applied Optics, 1996. **35**(13): p. 2304-2314.
10. Comelli, D., et al., *In vivo time-resolved reflectance spectroscopy of the human forehead.* Applied Optics, 2007. **46**(10): p. 1717-1725.
11. Ohmae, E., et al., *Cerebral hemodynamics evaluation by near-infrared time-resolved spectroscopy: correlation with simultaneous positron emission tomography measurements.* Neuroimage, 2006. **29**(3): p. 697-705.

12. Fantini, S., et al., *Frequency-domain multichannel optical detector for noninvasive tissue spectroscopy and oximetry.* Optical Engineering, 1995. **34**(1): p. 32-42.
13. Franceschini, M.A., et al., *Assessment of infant brain development with frequency-domain near-infrared spectroscopy.* Pediatric research, 2007. **61**: p. 546-551.
14. Zhao, J., et al., *In vivo determination of the optical properties of infant brain using frequency-domain near-infrared spectroscopy.* Journal of Biomedical Optics, 2005. **10**(2): p. 024028-0240287.
15. Hallacoglu, B., et al., *Absolute measurement of cerebral optical coefficients, hemoglobin concentration and oxygen saturation in old and young adults with near-infrared spectroscopy.* Journal of Biomedical Optics, 2012. **17**(8): p. 0814061-0814068.
16. Grant, P.E., et al., *Increased cerebral blood volume and oxygen consumption in neonatal brain injury.* Journal of Cerebral Blood Flow & Metabolism, 2009. **29**(10): p. 1704-1713.
17. Ijichi, S., et al., *Developmental changes of optical properties in neonates determined by near-infrared time-resolved spectroscopy.* Pediatric research, 2005. **58**(3): p. 568-573.
18. Yokose, N., et al., *Bedside monitoring of cerebral blood oxygenation and hemodynamics after aneurysmal subarachnoid hemorrhage by quantitative time-resolved near-infrared spectroscopy.* World neurosurgery, 2010. **73**(5): p. 508-513.
19. Ohmae, E., et al., *Clinical evaluation of time-resolved spectroscopy by measuring cerebral hemodynamics during cardiopulmonary bypass surgery.* Journal of Biomedical Optics, 2007. **12**(6): p. 062112-062112-9.
20. Swartling, J., J.S. Dam, and S. Andersson-Engels, *Comparison of spatially and temporally resolved diffuse-reflectance measurement systems for determination of biomedical optical properties.* Applied Optics, 2003. **42**(22): p. 4612-4620.
21. Francis, R., et al., *NIR light propagation in a digital head model for traumatic brain injury (TBI).* Biomedical optics express, 2015. **6**(9): p. 3256-3267.
22. Bonnéry, C., et al., *Changes in diffusion path length with old age in diffuse optical tomography.* Journal of Biomedical Optics, 2012. **17**(5): p. 056002.
23. Scholkmann, F. and M. Wolf, *General equation for the differential pathlength factor of the frontal human head depending on wavelength and age.* Journal of Biomedical Optics, 2013. **18**(10): p. 105004.